

Bond formation kinetics affects self-assembly directed by ligand–receptor interactions^{a)}

S. J. Bachmann[†], M. Petizon[†], B. M. Mognetti^{*1}

Université Libre de Bruxelles (ULB), Interdisciplinary Center for Nonlinear Phenomena and Complex Systems & Service de Physique des Systèmes Complexes et Mécanique Statistique, Campus Plaine, CP 231, Blvd du Triomphe, B-1050 Brussels, Belgium.

In this paper we study aggregation kinetics in systems of particles functionalised by complementary linkers. Most of the coarse-grained models currently employed to study large-scale self-assembly of these systems rely on effective potentials between particles as calculated using equilibrium statistical mechanics. In these approaches the kinetic aspects underlying the formation of inter-particle linkages are neglected. We show how the rate at which supramolecular linkages form drastically changes the self-assembly pathway. In order to do this we develop a method that combines Brownian dynamics simulations with a Gillespie algorithm accounting for the evolution of inter-particle linkages. If compared with dynamics based on effective potentials, an explicit description of inter-particle linkages results in aggregates that in the early stages of self-assembly have a lower valency. Relaxation towards equilibrium is hampered by the time required to break existing linkages within one cluster and to reorient them toward free particles. This effect is more important at low temperature and high particle diffusion constant. Our results highlight the importance of including kinetic rates into coarse-grained descriptions of ligand–receptor systems.

^{a)} [†]These authors contributed equally to this work; ^{*}corresponding author: bmognett@ulb.ac.be

I. INTRODUCTION

Supramolecular interactions mediated by ligand–receptor constructs are broadly used in nanoscience, for instance, to design systems that self–assemble^{1–3} or to develop materials for drug–delivery⁴ and remote–sensing⁵ applications. Ligand–receptor interactions also control many biological functionalities including cell signalling and inter–membrane adhesion.

Modelling supramolecular interactions is challenging because it requires mapping atomistic details into coarse-grained representations of complex systems such as colloids^{6–19} or polymers^{20–22} functionalised by reactive complexes. However, simplified models are necessary to access the time and length scales necessary to study, for instance, selectivity in systems of functionalised nanoparticles,²³ or self-assembly of large crystalline structures.^{12,13}

A popular method of coarse-graining ligand–receptor systems relies on the use of effective, state-dependent, potentials. In this approach complex unit components, such as colloids functionalised by many polymeric strands, are mapped into point–like particles interacting *via* effective interactions (see Fig. 1a). Effective interactions are calculated by sampling all possible micro–states involving two^{15–18,24} (or more¹⁴) particles at fixed distances.^{7,8,11–13,25} Effective potentials have been largely used to study soft materials (e.g., in the blob representation of polymers²⁶) and biological processes (e.g., protein aggregation²⁷).

In this paper we question the use of effective potentials to study self-assembly of particles functionalised by ligands with mobile tethering point. We show that considering the finite rates at which supramolecular linkages form, drastically changes self-assembly pathway. The effect is more important at low temperatures where, already at the stage when only clusters with few particles are formed, most of the ligands are engaged in supramolecular linkages. The scarcity of free ligands hampers the formation of new bonds and therefore the growth of early–formed aggregates. Such reaction–limited dynamics not only slows down self-assembly but also results in aggregates with low coordination number even at late stages of aggregations. We classify different self-assembly kinetics using an experimentally accessible adimensional parameter relating the time taken by particles to diffuse over a distance equal to the size of the ligands with the average time required to form supramolecular linkages.

The manuscript is organised as follows: In Sec. II we introduce the model and calculate the rates of forming/breaking supramolecular linkages. In Sec. III we present and validate our

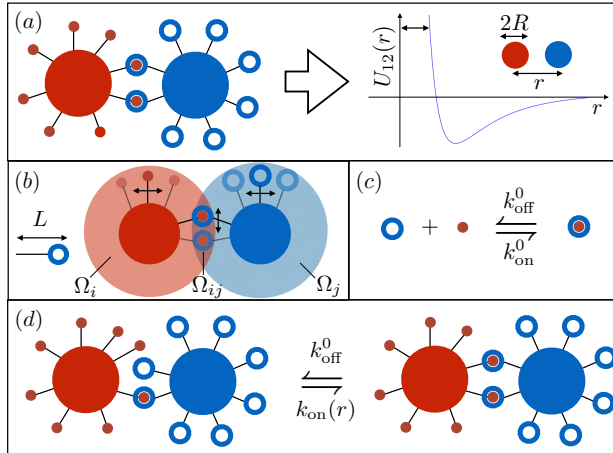


FIG. 1. (a) Particles functionalised with ligand-receptor constructs are usually modelled by means of effective potentials U_{12} that are calculated by sampling over all possible inter-particle linkages. (b) Considering ideal mobile linkers, Ω_i (Ω_j) and Ω_{ij} are the volumes of the configurational space available to free and hybridised linkers.¹⁴ The reaction rates of free linkers in solution (c) are modified in the case of tethered constructs (d).

simulation methods. In Sec. IV simulation results are reported while in Sec. V our findings are discussed.

II. THE MODEL

We study hard spheres of radius R functionalized with N linkers carrying reactive complexes that selectively bind (see Fig. 1). In particular we consider a binary system made of two types of particles (A and \bar{A}) functionalized by complementary linkers (α and $\bar{\alpha}$, respectively). When two complexes hybridize an inter-particle linkage (*bridge*) forms.

As found in systems of functionalized emulsions^{28–30} and lipid bilayers,^{31–34} as well as when modelling adhesion between biological membranes,³⁵ we consider linkers that can freely diffuse on particle surfaces (Fig. 1b). In particular, we use the model presented in Ref.¹⁴, itself inspired by the experiments of van der Meulen and Leunissen in which solid colloids are coated with lipid bilayers.³¹ Linkers are made of double-stranded DNA anchored to the membrane by cholesterol anchors immersed into the bilayer, and are tipped by reactive complexes like, for instance, short sequences of single-stranded DNA. In our modelling, such constructs are mapped into thin rigid rods of length L terminated by reactive points that

bind with a complementary partner under hybridization conditions (see Fig. 1a). We neglect rod-rod interactions but account for steric repulsions between hard particles and rods.¹⁴ In this work we consider $N_p = 100$ particles of radius $R = 5 \cdot L$.¹⁴

In the following we denote particle spatial coordinates by $\{\mathbf{r}\}$ ($\{\mathbf{r}\} = \mathbf{r}_1, \mathbf{r}_2, \dots, \mathbf{r}_{N_p}$). The hybridisation free energy of forming a given bridge between particles i and j at fixed $\{\mathbf{r}\}$ is¹⁴

$$e^{-\beta\Delta G_{ij}(\{\mathbf{r}\})} = \left(\frac{\Omega_{ij}(\{\mathbf{r}\})}{\rho_{\ominus}\Omega_i(\{\mathbf{r}\})\Omega_j(\{\mathbf{r}\})} \right) e^{-\beta\Delta G_0} \quad (1)$$

where ΔG_0 is the hybridisation free energy of the reactive complexes when free in solution and ρ_{\ominus} is the standard concentration ($\rho_{\ominus} = 1 \text{ M}$). In Eq. 1, Ω_i and Ω_{ij} are the configurational space volumes of a free linker on particle i and of a bridge linking particle i with particle j (see Fig. 1b). Note that Ω_i depends on the positions \mathbf{r}_j of all particles j that can be touched by linkers tethered on i while, in the low L/R limit, Ω_{ij} is only a function of \mathbf{r}_i and \mathbf{r}_j (see Appendix A).

The linkage dynamics at given $\{\mathbf{r}\}$ is specified by $k_{\text{on}}^{(i,j)}$ and $k_{\text{off}}^{(i,j)}$: The rates at which bridges between particles i and j are formed and broken, respectively (see Fig. 1d). Using Eq. 1 and following Ref.³⁶ it can be shown that

$$k_{\text{on}}^{(i,j)} = \left(\frac{\Omega_{ij}(\{\mathbf{r}\})}{\Omega_i(\{\mathbf{r}\})\Omega_j(\{\mathbf{r}\})} \right) k_{\text{on}}^0 \quad k_{\text{off}}^{(i,j)} = \rho_{\ominus} e^{\beta\Delta G_0} k_{\text{on}}^0, \quad (2)$$

where k_{on}^0 is the *on* rate of reactive complexes when free in solution (see Fig. 1c), and we have assumed that the *off* rates of free and tethered complexes are the same.³⁶ Eqs. 2 allow to calculate $k_{\text{on}}^{(i,j)}$ and $k_{\text{off}}^{(i,j)}$ for a given configuration $\{\mathbf{r}\}$ as a function of k_{on}^0 . Note that Eqs. 2 neglect the fact that the mobility of linkers moving on particle surfaces is finite.³¹ This is a fair approximation in the case of DNA at low temperatures, where the kinetics is dominated by DNA denaturation.³⁶

Given the hybridisation free energies of single bond formation (Eq. 1), we can derive the partition function of the system (Z).¹⁴ At finite particle density the configurational space available to free linkers is reduced by the presence of neighbouring colloids. This phase space contraction contributes to the partition function as (see Eq. 5)¹⁴

$$Z_{\text{excl}}(\{\mathbf{r}\}) = \prod_{i=1}^{N_p} \left(\frac{\Omega_i(\{\mathbf{r}\})}{\Omega_0} \right)^N, \quad (3)$$

where Ω_0 is the configurational space available to a free linker moving on an isolated colloid. Defining by n_{ij} the number of bridges between particle i and j ($1 \leq i < j \leq N_p$ and

$\Delta G_0 < \infty$), the contribution to the partition function due to bridges at fixed $\{n_{ij}\}$ and $\{\mathbf{r}\}$ is written as^{14,22?, 23}

$$\begin{aligned} Z_{\text{att}}(\{\mathbf{r}\}, \{n_{ij}\}) &= \prod_{i=1}^{N_p} \frac{N!}{n_i! \prod_q n_{iq}!} \cdot \prod_{k<j} [n_{kj}! e^{-\beta \Delta G_{kj}(\{\mathbf{r}\}) n_{kj}}] \\ &= \prod_{i=1}^{N_p} \frac{N!}{n_i!} \cdot \prod_{k<j} \frac{e^{-\beta \Delta G_{kj}(\{\mathbf{r}\}) n_{kj}}}{n_{kj}!} \end{aligned} \quad (4)$$

where n_i is the number of free linkers on particle i ($n_i = N - \sum_j n_{ij}$). In the first line of Eq. 4, $N!/(n_i! \prod_q n_{iq}!)$ is the number of ways of partitioning N linkers into N_p groups $\{n_{ip}\}$ ($p = 1, \dots, N_p$) within which they are indistinguishable, while $n_{kj}!$ is the number of ways of making n_{kj} bridges starting from n_{kj} complementary pairs. Finally the partition function of a N_p particle system is obtained using Z_{excl} and Z_{att} , defined above, and summing over all possible $\{n_{ij}\}$ and $\{\mathbf{r}\}$ ³⁷

$$\begin{aligned} Z &= \frac{1}{(N_p/2)!^2} \int d\{\mathbf{r}\} e^{-\beta V(\{\mathbf{r}\})} Z_{\text{excl}}(\{\mathbf{r}\}) \sum_{\{n_{kj}\}} Z_{\text{att}}(\{\mathbf{r}\}, \{n_{kj}\}) \quad (5) \\ &= \int \frac{d\{\mathbf{r}\} e^{-\beta V(\{\mathbf{r}\})}}{(N_p/2)!^2} \sum_{\{n_{kj}\}} \prod_{i=1}^{N_p} \left(\frac{\Omega_i(\{\mathbf{r}\})}{\Omega_0} \right)^N \frac{N!}{n_i!} \prod_{k<j} \frac{e^{-\beta \Delta G_{kj}(\{\mathbf{r}\}) n_{kj}}}{n_{kj}!}. \end{aligned}$$

In the latter expression the sum is taken over all possible bridges ($\{n_{ij}\}$) at given $\{\mathbf{r}\}$ (in particular $n_{ij} > 0$ only if i and j are complementary and $0 \leq n_i, n_{ij} \leq N$). $V(\{\mathbf{r}\})$ is used to regularise hard-core interactions and has been taken equal to the sum of pairwise repulsions between two particles functionalized by 500 inert linkers of length $L_{\text{inert}} = 0.75L$. This choice does not affect the conclusions of the paper and, if compared to sharper potentials, allowed to use larger integration steps.

In Ref.¹⁴ a saddle point approximation is used to replace the sum over $\{n_{ij}\}$ in Eq. 5 by their most probable values \bar{n}_{ij} . In particular in the large N limit it can be shown that

$$Z = \int d\{\mathbf{r}\} e^{-\beta \mathcal{F}(\bar{n}_{ij}, \beta \Delta G_{ij}(\{\mathbf{r}\}), \Omega_i(\{\mathbf{r}\}))} \quad (6)$$

with \mathcal{F} defined by the integrand of Eq. 5 and the most probable numbers of linkages \bar{n}_{ij} satisfying chemical equilibrium equations¹⁴

$$\bar{n}_{ij} = (N - \sum_p \bar{n}_{ip})(N - \sum_q \bar{n}_{jq}) e^{-\beta \Delta G_{ij}(\{\mathbf{r}\})}. \quad (7)$$

If $\bar{n}_i = N - \sum_p \bar{n}_{ip}$ the previous equations can be rewritten as

$$\bar{n}_i = \frac{N}{1 + \sum_p \bar{n}_p \exp[-\beta \Delta G_{ip}(\{\mathbf{r}\})]}$$

that allow calculating \bar{n}_i and \bar{n}_{ij} using self-consistent iteration methods.²⁵ In Ref.¹⁴ Eqs. 6 and 7, together with portable expressions of $\mathcal{F}(\bar{n})$,^{38,39} have been used to sample suspensions of functionalized particles by means of Monte Carlo algorithms in which the stationary numbers of linkages are calculated at each particle displacement using Eq. 7. Note that because Eqs. 7 couple all $\{\bar{n}_{ij}\}$ connecting particles that belong to the same cluster, $\mathcal{F}(\bar{n})$ is multibody. The multibody nature of \mathcal{F} is also due to the fact that $\Omega_i(\{\mathbf{r}\})$, controlling the formation of bridges between i and j (Eq. 1), is function of all neighboring particles interacting with i (see Appendix A).

In this work we study self-assembly kinetics by means of Brownian dynamics. We use an *implicit-linker method* in which forces between particles at given spatial configuration $\{\mathbf{r}\}$ are evaluated by means of Eqs. 6 and 7. In this scheme the number of linkers between particles are always taken equal to their most probable value (Eq. 7) resulting in forces ($\bar{\mathbf{f}}$) that are only function of $\{\mathbf{r}\}$. This is equivalent to having infinite *on* rates ($k_{\text{on}}^0 = \infty$). We also develop an *explicit-linker method* in which we do not use Eq. 7 to instantaneously relax the numbers of bridges to their most probable values but treat n_{ij} as dynamic variables. In this case forces \mathbf{f} are evaluated using the integrand of Eq. 5 at given values of $\{n_{ij}\}$. The number of bridges $\{n_{ij}\}$ is updated using the Gillespie algorithm⁴⁰ fed by *on* and *off* rates calculated using Eq. 2.

We first calculate the force acting on particle i in the implicit-linker method ($\bar{\mathbf{f}}_i$). Using Eqs. 5, 6 and 7 we obtain (defining $\nabla_i = \partial/\partial\mathbf{r}_i$)⁴¹

$$\begin{aligned}\bar{\mathbf{f}}_i &= -\nabla_i \mathcal{F}(\bar{n}_{pq}, \beta\Delta G_{pq}(\{\mathbf{r}\}), \Omega_p(\{\mathbf{r}\})) \\ &= -\sum_{p<q} \nabla_i \bar{n}_{pq} \frac{\partial \mathcal{F}(\bar{n}_{pq}, \beta\Delta G_{pq}(\{\mathbf{r}\}), \Omega_p(\{\mathbf{r}\}))}{\partial n_{pq}} - \nabla_i V(\{\mathbf{r}\}) \\ &\quad - \sum_{p<q} \nabla_i \Delta G_{pq}(\{\mathbf{r}\}) \frac{\partial \mathcal{F}(\bar{n}_{pq}, \beta\Delta G_{pq}(\{\mathbf{r}\}), \Omega_p(\{\mathbf{r}\}))}{\partial \Delta G_{pq}(\{\mathbf{r}\})} \\ &\quad - \sum_p \nabla_i \Omega_p(\{\mathbf{r}\}) \frac{\partial \mathcal{F}(\bar{n}_{pq}, \beta\Delta G_{pq}(\{\mathbf{r}\}), \Omega_p(\{\mathbf{r}\}))}{\partial \Omega_p(\{\mathbf{r}\})}.\end{aligned}\tag{8}$$

Noting that the saddle-point condition (Eq. 7) is written as $\partial \mathcal{F}(\bar{n}_{pq})/\partial n_{ij} = 0$ and using the explicit form of \mathcal{F} as obtained comparing Eq. 5 with Eq. 6 we find the following expression⁴¹

$$\bar{\mathbf{f}}_i = -\sum_{p<q} \bar{n}_{pq} \nabla_i \Delta G_{pq}(\{\mathbf{r}\}) + Nk_B T \sum_p \frac{\nabla_i \Omega_p(\{\mathbf{r}\})}{\Omega_p(\{\mathbf{r}\})} - \nabla_i V(\{\mathbf{r}\}).\tag{9}$$

The expression of the forces in case of explicit-linker dynamics is identical to Eq. 9 when \bar{n}_{ij} are replaced by n_{ij} . In explicit-linker dynamics particle displacements are done at n_{ij}

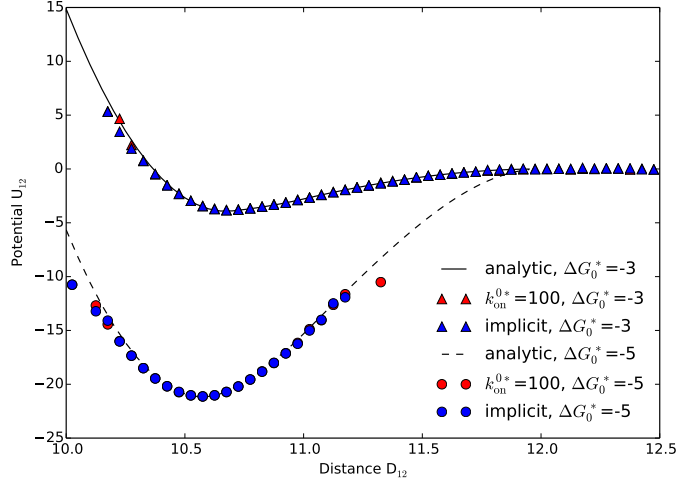


FIG. 2. Effective pair interactions as calculated using the **implicit-linker** (blue symbols) and the **explicit-linker method** (red symbols) as a function of the distance between centres of mass (D_{12}). Curves refer to analytic values of U_{12} calculated using Eq. 6. Two values of ΔG_0^* have been used. The simulated potentials have been shifted to match analytic predictions at $2R^* + 2$ when $\Delta G_0^* = -3$, and at r_{\min}^* (with r_{\min}^* minimum of U_{12}) when $\Delta G_0^* = -5$. The same conclusions are reached when using different values of Δt^* .

constant and the first variation in the second line of Eq. 8 disappears resulting in

$$\mathbf{f}_i = - \sum_{p < q} n_{pq} \nabla_i \Delta G_{pq}(\{\mathbf{r}\}) + N k_B T \sum_p \frac{\nabla_i \Omega_p(\{\mathbf{r}\})}{\Omega_p(\{\mathbf{r}\})} - \nabla_i V(\{\mathbf{r}\}). \quad (10)$$

Eqs. 9 and 10 will be used to develop Brownian dynamics simulations as described in Sec. III. A computationally efficient decomposition of Eqs. 9 and 10, adapted to the system studied in this work, is reported in Appendix A.

III. SIMULATION METHODS

Chosen simulation unit length and time are L and L^2/D , where D is the diffusion coefficient. In particular the adimensional *on* rate of free complexes in solution is defined as $k_{\text{on}}^{0*} = k_{\text{on}}^0/(LD)$. Note that k_{on}^{0*} can be interpreted as the ratio between the time taken by particles to diffuse a length equal to L and the average time for a reaction between complexes in solution at number density equal to $1/L^3$ to happen. In the following, all quantities tagged by $*$ are meant to be in simulation units. For instance, hybridisation free energies of

tethered linkers (Eq. 1) become

$$\beta\Delta G_{ij}(\{\mathbf{r}^*\}) = \Delta G_0^* - \log\left(\frac{\Omega_{ij}^*(\{\mathbf{r}^*\})}{\Omega_i^*(\{\mathbf{r}^*\})\Omega_j^*(\{\mathbf{r}^*\})}\right)$$

$$\Delta G_0^* = \beta\Delta G_0 - \log\frac{1}{\rho_\ominus L^3}.$$

At each cycle of our algorithms we first update the number of bridges between particles at given $\{\mathbf{r}\}$. In the implicit-linker method we numerically solve Eq. 7 and calculate $\bar{n}_{ij}(\{\mathbf{r}\})$. This is done by fixed point iterations as reported in Ref.²⁵ and¹⁴. In the explicit-linker method we update $\{n_{ij}\}$ using the Gillespie algorithm.⁴⁰ We calculate the propensity of making/breaking a bridge between particles i and j as (see Eq. 2)

$$a_{\text{on}}^{(i,j)} = n_i n_j k_{\text{on}}^{(i,j)} \quad a_{\text{off}}^{(i,j)} = n_{ij} k_{\text{off}}^{(i,j)} \quad (11)$$

and define $a_{\text{tot}} = \sum_{i<j} a_{\text{on}}^{(i,j)} + a_{\text{off}}^{(i,j)}$. We sample the next reaction as well as the time interval for it to happen (τ). In particular we add (remove) a bridge between particles i and j with probability $a_{\text{on}}^{(i,j)}/a_{\text{tot}}$ ($a_{\text{off}}^{(i,j)}/a_{\text{tot}}$). Note that at this stage we both sample the type of reaction and the particles involved. τ is calculated by sampling from the probability distribution function $p(\tau) = a_{\text{tot}} \exp[-a_{\text{tot}}\tau]$.⁴⁰ We then update the propensity matrices (Eqs. 11) and repeat the entire process until the cumulative time interval of all reactions becomes bigger than the integration step Δt^* used in the Brownian dynamics integration (see below). We note that more efficient algorithms, capable of updating the number of different “species” (n_{ij}) at time $t^* + \Delta t^*$ in one go, have been proposed.^{42–44} Testing the efficiency of these schemes for the present system goes beyond the scope of this work.

The second part of the algorithms is common to the two methods and consists in a Brownian dynamics step in which particles’ centres of mass are evolved according to⁴⁵

$$\mathbf{r}_i^*(t + \Delta t) = \mathbf{r}_i^*(t) + \beta \mathbf{F}_i L \Delta t^* + \sqrt{2\Delta t^*} \mathcal{N}(0, 1) \quad (12)$$

with $\mathbf{F}_i = \bar{\mathbf{f}}_i$ (Eq. 9 and Appendix A) when using the implicit-linker method and $\mathbf{F}_i = \mathbf{f}_i$ (Eq. 10 and Appendix A) when using the explicit-linker method. $\mathcal{N}(0, 1)$ is a normally distributed random variable with zero mean and variance equal to one. In this work we use $\Delta t^* = 0.001$. Such value guaranteed affordable simulations and did not produce numerical instabilities usually found at high Δt^* . We also verified the fairness of the algorithm at small values of Δt^* ($\Delta t^* = 10^{-6} - 10^{-4}$) by comparing effective pair interactions as done in

Fig. 2.

The flow charts of the two algorithms are summarised below:

- **Implicit–linker method**

- while $t^* < t_{\text{tot}}^*$
 - * for given $\{\mathbf{r}^*(t^*)\}$ calculate \bar{n}_{ij} using Eq. 7
 - * calculate $\{\mathbf{r}^*(t^* + \Delta t^*)\}$ using Eq. 12 and $\mathbf{F}_i = \bar{\mathbf{f}}_i$
 - * $t^* \rightarrow t^* + \Delta t^*$

- **Explicit–linker method**

- while $t^* < t_{\text{tot}}^*$
 - * for given $\{\mathbf{r}^*(t^*)\}$ calculate $a_{\text{off}}^{(i,j)}$ and $a_{\text{on}}^{(i,j)}$ using Eqs. 11 and Eqs. 2
 - * while $\bar{t}^* < \Delta t^*$
 - sample the next reaction and the time interval τ
 - upgrade $\{n_{ij}\}$, $a_{\text{off}}^{(i,j)}$, and $a_{\text{on}}^{(i,j)}$
 - $\bar{t}^* \rightarrow \bar{t}^* + \tau$
 - * calculate $\{\mathbf{r}^*(t^* + \Delta t^*)\}$ using Eq. 12 and $\mathbf{F}_i = \mathbf{f}_i$
 - * $t^* \rightarrow t^* + \Delta t^*$

In the $\Delta t^* \rightarrow 0$ limit, both methods satisfy detailed balance with respect to the distribution function $p(\{\mathbf{r}\}) \sim \exp[-\beta\mathcal{F}(\{n_{ij}\}, \{\mathbf{r}\})]$ (Eq. 6).⁴⁶ In particular, they should reproduce the same results when used to sample equilibrium properties of the system. This has been verified in Fig. 2 where, similar to what done in experiments with particles in optical traps,¹⁸ we calculate effective pair interactions (U_{12}) by means of Boltzmann inversion.¹⁸ For two different values of ΔG_0^* and for $k_{\text{on}}^{0*} = 100$ we verify that the two dynamics reproduce the same U_{12} that also agree with the analytic results calculated using Eq. 6. Note that in Fig. 2 we have chosen the lowest value of k_{on}^{0*} used in the work. This is the most subtle case in view of the fact that, at least for systems with two particles, the two dynamics become equivalent in the high k_{on}^{0*} limit.

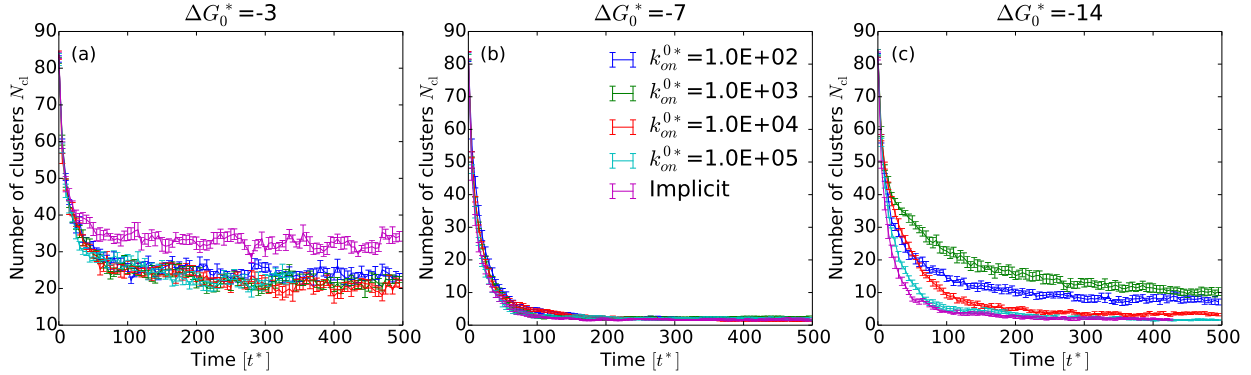


FIG. 3. Number of clusters *versus* simulation time at three different values of ΔG_0^* . For explicit-linker dynamics at low values of k_{on}^{0*} and $\Delta G_0^* = -14$ particle aggregation is arrested.

IV. SELF-ASSEMBLY KINETICS

We simulate suspensions of $N_p = 100$ colloids at packing fraction of 0.1 starting from initial configurations in which particles are randomly distributed in the simulation box with periodic boundary conditions. We compare implicit-linker with explicit-linker simulations with k_{on}^{0*} encompassing four orders of magnitudes. Using the Stokes-Einstein equation for the diffusion constants of spherical particles through water and $k_{\text{on}}^0 = 10^6 / (\text{M}\cdot\text{s})$, we estimate $k_{\text{on}}^{0*} \approx 10^{-1} - 10^0$ for DNA coated colloids with radii ranging from 100 nm to 1000 nm. This value is smaller than what considered in our study (see Figs. 3 and 5) because simulations at low values of k_{on}^{0*} are more expensive. Due to the fact that the kinetic bottlenecks described in this work are more severe at low k_{on}^{0*} , our results highlight the importance of considering such effects in real experiments. Moreover k_{on}^{0*} can be tuned across several orders of magnitude using other reactive complexes than DNA.⁴⁷ In our simulations each data set has been obtained averaging over ten independent runs. When using Python, each run required on average 7-14 days of an AMD Opteron 6274 CPU (2.2 GHz).

In Fig. 3 we report the time evolution of the total number of clusters (N_{cl}). At $t^* = 0$, N_{cl} is comparable with N_p . As aggregates start to form the number of clusters decreases until reaching a steady value. For $\Delta G_0^* = -3$, N_{cl} tends to $\approx 20 - 30$ (see Fig. 3a). In this case a rich gas phase, consisting of around 10-20 singlets (see SI Fig. S1a), few dimers and some trimers (see SI Fig. S2a,d), coexists with bigger clusters made of around 15-30 particles (see SI Fig. S3a). These aggregates have a very low coordination number ($\langle z \rangle \approx 1.9 - 2.5$, see

SI Fig. S4a) and resemble branched colloidal chains (see Fig. 4). Interestingly, in recent experiments of solid particles functionalised by mobile linkers colloidal chains have been observed in a broad range of temperatures.³¹

Surprisingly in Fig. 3a results obtained with the two different simulation methods do not perfectly agree. First we note that for $\Delta G_0^* = -3$ particles interact weakly (see Fig. 2) resulting in reversible growth dynamics. We also note that particle detachment rates are smaller when k_{off} is finite than in implicit-linker dynamics. Moreover, at fixed number of bridges, particles cross-linked by explicit linkers are closer than in the implicit linker case (note that the configurational free energy, Eq. 1, diverges when the distance between particles is $2(R + L)$). It may be that, in explicit linker dynamics, particles can diffuse at the interface of aggregates long enough to stabilise themselves by binding a second colloid, most likely belonging to the same cluster. This mechanism may explain why aggregates grow faster when k_{off} is finite. This hypothesis is supported by SI Fig. S4a showing that the average coordination number of aggregates is bigger in explicit-linker simulations. In SI Fig. S5 we repeated simulations using colloidal suspensions at lower density. In this case, smaller clusters are formed and the discrepancy between implicit and explicit simulations decreases. In SI Fig. S6 and S7 we test the precision of the saddle-point approximation by increasing the number of linkers to $N = 100$. First, in SI Fig. S6 we fine-tune the hybridisation free energy ΔG_0^* for the $N = 100$ model resulting in a pair potential comparable with the $N = 40$ model and $\Delta G_0^* = -3$. Using this model, in Fig. S7 we calculate the number of clusters versus time. The deviation between the two dynamics in Fig. S7 is comparable with what has been found in Fig. 3a. This shows that the saddle point approximation is not responsible for the discrepancies between implicit and explicit methods at $\Delta G_0^* = -3$. A more detailed study of multibody effects in the reversible limit at different k_{on}^{0*} deserves further investigations.

For $\Delta G_0^* \leq -7$ and for implicit-linker simulations particle attachment becomes irreversible and the gas phase tends to disappear. In particular, for times bigger than $t^* \approx 100 - 150$ all particles are found in few clusters as expected deep in the coexisting region (see Figs. 3b and 3c). At intermediate values of ΔG_0^* ($\Delta G_0^* = -7$ in Fig. 3b) the number of clusters calculated using explicit-linker dynamics matches implicit-linker results for any k_{on}^{0*} . The same holds true for the number of singlets (see SI Fig. S1b), the number of dimers and trimers (see SI Fig. S2b,e), the size of the biggest cluster (see SI Fig. S3b), and for the average coordination

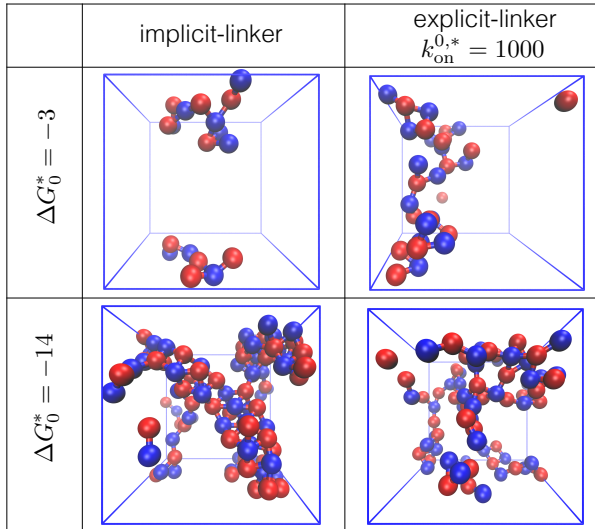


FIG. 4. Final simulation snapshots showing the biggest cluster. For clarity particles in the gas phase, including smaller clusters, have not been reported. For $\Delta G_0^* = -14$ the average coordination number is $\langle z \rangle \approx 2$ and $\langle z \rangle \approx 4$ for the explicit-linker and the implicit-linker method, respectively (see Fig. 5).

number of the biggest cluster (see SI Fig. S4b).

Intriguingly the two methods no longer agree at the lowest value of ΔG_0^* considered ($\Delta G_0^* = -14$ in Fig. 3c) where explicit-linker simulations at low $k_{\text{on}}^{0,*}$ fail to assemble a single cluster. In particular we find that for $k_{\text{on}}^{0,*} < 10^4$ significant amounts of dimers and trimers are still present at the end of the simulations (see SI Fig. S2). This implies that at low ΔG_0^* self-assembly is reaction-limited: The effective rate of attaching monomers to extended clusters is smaller than the same quantity at higher values of ΔG_0^* (see discussion in Sec. V). This is confirmed by SI Fig. S3c that reports the size of the biggest clusters.

The typical morphologies of the aggregates are also very different when applying the two methods. This is shown in Fig. 5 where we study the average coordination number of the biggest cluster ($\langle z \rangle$) in the system *versus* simulation time for $\Delta G_0^* = -14$. For explicit-linker dynamics, especially at low values of $k_{\text{on}}^{0,*}$, $\langle z \rangle$ increases very slowly and remains almost constant ($\langle z \rangle \approx 2$) during all simulations. The typical biggest clusters for $\Delta G_0^* = -14$ are reported in the second row of Fig. 4. For explicit-linker schemes we see that aggregates remain chain like even when they start to percolate through the simulation box. This proves that explicitly accounting for rate formation of supramolecular linkages not only slows down

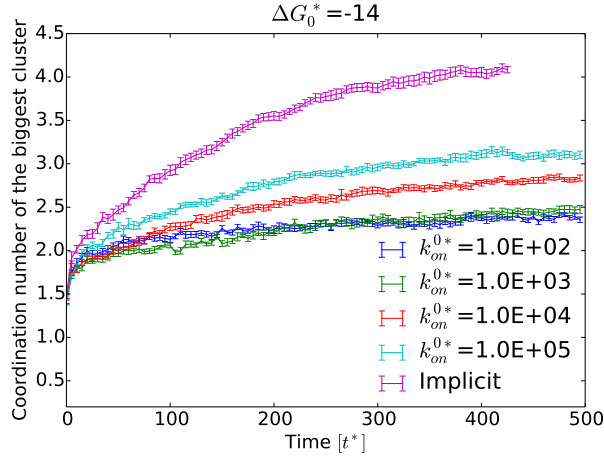


FIG. 5. Average valence ($\langle z \rangle$) of particles in the biggest cluster *versus* simulation time for $\Delta G_0^* = -14$. For explicit-linker simulations, valences tend to values slightly bigger than 2 as confirmed by Fig. 5.

self-assembly but also results in more open aggregates.

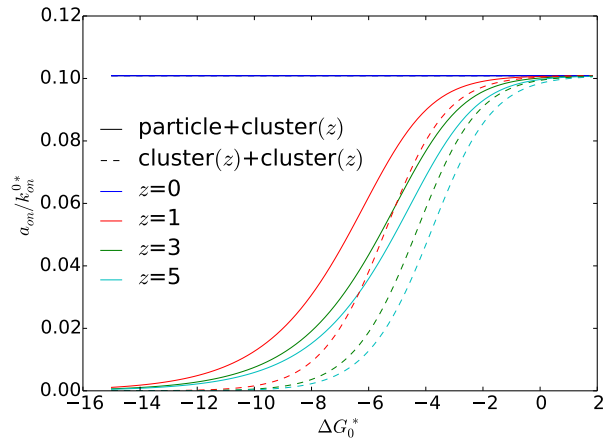


FIG. 6. Propensity (see Eq. 11) of attaching an isolated particle to an existing cluster (solid lines), and propensity of creating a new linkage between two particles embedded in the same cluster (dashed lines). In all calculations the distance between linkable particles has been taken equal to $2 \cdot R + L$ and z is the cluster coordination number.

V. DISCUSSION

Self-assembly of particles featuring explicit linkers is controlled by the finite time required by existing clusters to capture a new particle. When using effective interactions, a particle wiggling around a cluster is immediately stabilized by the outer shell of the aggregate. On the other hand, in the cases of models with explicit linker dynamics, available linkers on the clusters may not be fast enough to tie free particles letting them to diffuse away. As shown in Fig. 3 this is more relevant at low ΔG_0^* because less free linkers are available and the rates of breaking linkages becomes small (see Eq. 2). This has been rationalized in Fig. 6 (solid lines) where we calculate the propensity of attaching a singlet to a cluster as a function of ΔG_0^* . In this figure we first consider infinite clusters with valence equal to z and distance between bound particles equal to $2 \cdot R + L$ and calculate the number of linkages per particle at equilibrium (Eq. 7). We then use Eq. 11 to calculate the propensity of making a bridge between one particle in the cluster and a free particle placed at distance equal to $2 \cdot R + L$. While the propensity remains constant when linking two free particles ($z = 0$), in case of extended clusters it drastically drops to zero for $\Delta G_0^* \lesssim -10$. The effect is more important at high z due to the fact that less free linkers are available in the presence of more neighbors. This argument explains the results of Fig. 5: For $\Delta G_0^* = -14$ the propensity of attaching a singlet to an extended cluster become negligible and self-assembly is arrested. It also explains the fact that a significant amount of dimers is still present at the end of explicit-linker simulations (see SI Fig. S2c). Plots similar to Fig. 6 can be used to study the effects of changing the number of linkers N or the size of the particles R (see SI Fig. S8). Results similar to what is shown in Fig. 3 and Fig. 6 have been reported in a study of liposomes functionalized by two families of complementary DNA linkers.³⁶ In these systems inter-particle bridges compete with intra-particle loops resulting in a slow-down of aggregation at low temperature.³⁶ Linker sequestration may also underlay the findings of Ref.⁴⁸ in which smart emulsions are used to adsorb controllable amounts of colloids without the need of reaching structural arrest.

Dashed lines in Fig. 6 show the propensities of linking two particles, both of them belonging to a cluster with coordination number equal to z (see Eq. 11). Also in this case a_{on} goes to zero at low ΔG_0^* . However now the effect is more important in view of the fact that both particles feature linkers that are already engaged in pre-existing linkages. These results

explain the fact that in explicit-linker simulations chain-like structures do not fold onto themselves but persist until they percolate through the simulation box.

In conclusion we have studied self-assembly of particles functionalized by mobile ligands and have proven how accounting for linkage dynamics slows down colloid aggregation and results in clusters with low valence if compared with dynamics based on effective potentials. We believe our findings will be useful to develop coarse-grained models of supramolecular systems.

Acknowledgements SJB and BMM are supported by the Université Libre de Bruxelles (ULB). We acknowledge S. Angioletti-Uberti, L. Di Michele, P. Gaspard, and S. Napolitano for discussions. We acknowledge an anonymous reviewer for suggesting a more direct derivation of Eq. A7 than what was presented in an early version of the manuscript. Computational resources have been provided by the Consortium des Équipements de Calcul Intensif (CÉCI), funded by the Fonds de la Recherche Scientifique de Belgique (F.R.S.-FNRS) under Grant No. 2.5020.11.

Appendix A: Explicit calculation of \mathbf{f}_i and $\bar{\mathbf{f}}_i$

In this appendix we further develop Eqs. 10 and 9 and derive tractable expressions that can be used in the Brownian dynamics algorithms described in Sec. III. Using Eq. 1 and Eq. 10 we obtain

$$\beta\mathbf{f}_i = \sum_{p<q} n_{pq} \nabla_i \log \frac{\Omega_{pq}(\{\mathbf{r}\})}{\rho_{\ominus} \Omega_p(\{\mathbf{r}\}) \Omega_q(\{\mathbf{r}\})} + N \sum_p \frac{\nabla_i \Omega_p(\{\mathbf{r}\})}{\Omega_p(\{\mathbf{r}\})} - \beta \nabla_i V(\{\mathbf{r}\}) . \quad (\text{A1})$$

Using $N = n_i + \sum_j n_{ij}$ the previous relation can be further simplified as follows

$$\beta\mathbf{f}_i = \sum_{p<q} n_{pq} \frac{\nabla_i \Omega_{pq}(\{\mathbf{r}\})}{\Omega_{pq}(\{\mathbf{r}\})} + \sum_p n_p \frac{\nabla_i \Omega_p(\{\mathbf{r}\})}{\Omega_p(\{\mathbf{r}\})} - \beta \nabla_i V(\{\mathbf{r}\}) . \quad (\text{A2})$$

Eq. A2 is computationally more tractable than Eq. A1 because it allows calculating the force on particle i by cycling over all particles j that interact with i , either by forming bridges or by linker-colloid repulsion (see particles jointed to i by full curves in Fig. 7). Instead, attempting to evaluate the first term of Eq. A1 would also require to cycle on second-neighbour particles (see dashed lines in Fig. 7).

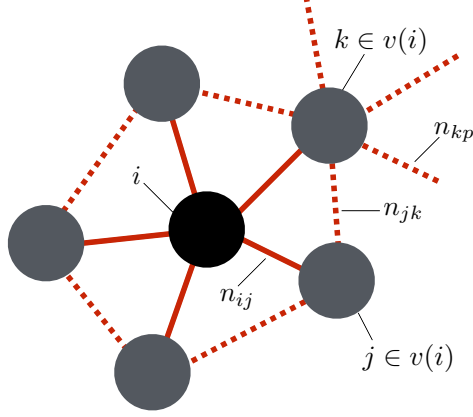


FIG. 7. The force acting on a given particle i is only due to particle j ($j \in v(i)$) that can directly interact with i (see Eq. A7).

In the limit in which the length of the mobile linkers is much smaller than the radius of the colloids ($L/R \ll 1$) the reactive end-points of the linkers (see Fig. 1) are uniformly distributed within the shell of radii R and $R + L$. In such limit Ω_i and Ω_{ij} (below denoted as w_{ij}) are equal to the volume available to free and hybridized end-points, respectively (the reliability of this approximation has been tested in the Supplementary Informations of Ref.¹⁴). If e_{ij} is the volume excluded to a free linker on particle i due to the presence of particle j , in the limit $L/R \ll 1$ we have

$$\Omega_i = \Omega_0 - \sum_{j \in v(i)} e_{ij} \quad \Omega_{ij} = w_{ij} \quad (\text{A3})$$

where $v(i)$ is the ensemble of particles which linkers can touch particle i (see Fig. 7) and $\Omega_0 = 4\pi R^2 L$. In Eq. A3 w_{ij} and e_{ij} are given by the following expressions

$$e_{ij}(r) = V_{\text{ovl}}(R + L, R, r) \quad (\text{A4})$$

$$w_{ij}(r) = V_{\text{ovl}}(R + L, R + L, r) - 2V_{\text{ovl}}(R + L, R, r), \quad (\text{A5})$$

where $r = |\mathbf{r}_i - \mathbf{r}_j|$ and $V_{\text{ovl}}(R_1, R_2, r)$ is the overlapping volume of two spheres of radius R_1 and R_2 placed at center-to-center distance equal to r

$$V_{\text{ovl}}(R_1, R_2, r) = \frac{\pi}{12r} (D - r)^2 (r^2 + 2rD - 3d^2), \quad (\text{A6})$$

with $d \leq r \leq D$, $d = |R_2 - R_1|$, and $D = R_1 + R_2$. Eqs. A5 and A6 imply that bridges can interact only with the two particles to which they are tethered. Inserting Eqs. A3 into

Eq. A2 we obtain our final result

$$\beta \mathbf{f}_i = \sum_j n_{ij} \frac{\nabla_i w_{ij}}{w_{ij}} - \sum_{j \in v(i)} \left[n_i \frac{\nabla_i e_{ij}}{\Omega_i} + n_j \frac{\nabla_i e_{ji}}{\Omega_j} \right] - \beta \nabla_i V(\{\mathbf{r}\}). \tag{A7}$$

Using Eq. A7 we calculate the force acting on a given particle i using a single loop over all particles belonging to $v(i)$ and tracking the values of $\Omega_j \forall j$. The expression of $\bar{\mathbf{f}}_i$ is obtained replacing n_{ij} and n_p with \bar{n}_{ij} and \bar{n}_p in Eq. A7.

REFERENCES

- ¹M. Kotera, J.-M. Lehn, and J.-P. Vigneron, “Self-assembled supramolecular rigid rods,” *J. Chem. Soc., Chem. Commun.*, 197–199 (1994).
- ²A. P. Alivisatos, K. P. Johnsson, X. Peng, T. E. Wilson, C. J. Loweth, M. P. Bruchez, and P. G. Schultz, “Organization of ‘nanocrystal molecules’ using DNA,” *Nature* **382**, 609 (1996).
- ³C. A. Mirkin, R. C. Letsinger, R. C. Mucic, and J. J. Storhoff, “A DNA-based method for rationally assembling nanoparticles into macroscopic materials,” *Nature* **382**, 607 (1996).
- ⁴C. B. Carlson, P. Mowery, R. M. Owen, E. C. Dykhuizen, and L. L. Kiessling, “Selective tumor cell targeting using low-affinity, multivalent interactions,” *ACS chemical biology* **2**, 119–127 (2007).
- ⁵T. A. Taton, C. A. Mirkin, and R. L. Letsinger, “Scanometric dna array detection with nanoparticle probes,” *Science* **289**, 1757–1760 (2000).
- ⁶C. W. Hsu, F. Sciortino, and F. W. Starr, “Theoretical description of a dna-linked nanoparticle self-assembly,” *Physical review letters* **105**, 055502 (2010).
- ⁷B. M. Mladek, J. Fornleitner, F. J. Martinez-Veracoechea, A. Dawid, and D. Frenkel, “Quantitative prediction of the phase diagram of dna-functionalized nanosized colloids,” *Physical review letters* **108**, 268301 (2012).
- ⁸B. M. Mladek, J. Fornleitner, F. J. Martinez-Veracoechea, A. Dawid, and D. Frenkel, “Procedure to construct a multi-scale coarse-grained model of dna-coated colloids from experimental data,” *Soft Matter* **9**, 7342–7355 (2013).
- ⁹F. J. Martinez-Veracoechea, B. Mladek, A. Tkachenko, and D. Frenkel, “Design rule for colloidal crystals of DNA-functionalized particles,” *Phys. Rev. Lett.* **107**, 045902 (2011).

- ¹⁰J. P. Lequeieu, D. M. Hinckley, and J. J. de Pablo, “A molecular view of dna-conjugated nanoparticle association energies,” *Soft Matter* (2015).
- ¹¹C. Knorowski and A. Travesset, “Self-assembly and crystallization of hairy (f-star) and dna-grafted nanocubes,” *Journal of the American Chemical Society* **136**, 653–659 (2014).
- ¹²S. Dhakal, K. L. Kohlstedt, G. C. Schatz, C. A. Mirkin, and M. Olvera De La Cruz, “Growth dynamics for dna-guided nanoparticle crystallization,” *ACS nano* **7**, 10948–10959 (2013).
- ¹³E. Auyeung, T. I. Li, A. J. Senesi, A. L. Schmucker, B. C. Pals, M. O. de La Cruz, and C. A. Mirkin, “Dna-mediated nanoparticle crystallization into wulff polyhedra,” *Nature* **505**, 73–77 (2014).
- ¹⁴S. Angioletti-Uberti, P. Varilly, B. M. Mognetti, and D. Frenkel, “Mobile linkers on dna-coated colloids: valency without patches,” *Phys. Rev. Lett.* **113**, 128303–128306 (2014).
- ¹⁵R. Dreyfus, M. E. Leunissen, R. Sha, A. Tkachenko, N. C. Seeman, D. J. Pine, and P. M. Chaikin, “Aggregation-disaggregation transition of DNA-coated colloids: Experiments and theory,” *Phys. Rev. E* **81**, 041404 (2010).
- ¹⁶R. Dreyfus, M. E. Leunissen, R. Sha, A. V. Tkachenko, N. C. Seeman, D. J. Pine, and P. M. Chaikin, “Simple quantitative model for the reversible association of DNA coated colloids,” *Phys. Rev. Lett.* **102**, 048301 (2009).
- ¹⁷M. E. Leunissen and D. Frenkel, “Numerical study of DNA-functionalized microparticles and nanoparticles: Explicit pair potentials and their implications for phase behavior,” *J. Chem. Phys.* **134**, 084702 (2011).
- ¹⁸W. B. Rogers and J. C. Crocker, “Direct measurements of dna-mediated colloidal interactions and their quantitative modeling,” *Proc. Natl. Acad. Sci. USA* **108**, 15687–15692 (2011), <http://www.pnas.org/content/108/38/15687.full.pdf+html>.
- ¹⁹Y. Ding and J. Mittal, “Insights into dna-mediated interparticle interactions from a coarse-grained model,” *The Journal of chemical physics* **141**, 184901 (2014).
- ²⁰R. De Gernier, T. Curk, G. V. Dubacheva, R. P. Richter, and B. M. Mognetti, “A new configurational bias scheme for sampling supramolecular structures,” *J. Chem. Phys.* **141**, 244909 (2014).
- ²¹G. V. Dubacheva, T. Curk, R. Auzély-Velty, D. Frenkel, and R. P. Richter, “Designing multivalent probes for tunable superselective targeting,” *Proc. Natl. Acad. Sci. USA* **112**, 5579–5584 (2015).

- ²²H. Xu and D. E. Shaw, “A simple model of multivalent adhesion and its application to influenza infection,” *Biophys. J.* **110**, 218–233 (2016).
- ²³F. J. Martinez-Veracoechea and D. Frenkel, “Designing super selectivity in multivalent nano-particle binding,” *Proc. Natl. Acad. Sci. USA* **108**, 10963–10968 (2011).
- ²⁴P. E. Theodorakis, C. Dellago, and G. Kahl, “A coarse-grained model for dna-functionalized spherical colloids, revisited: Effective pair potential from parallel replica simulations,” *The Journal of chemical physics* **138**, 025101 (2013).
- ²⁵P. Varilly, S. Angioletti-Uberti, B. Mognetti, and D. Frenkel, ““A general theory of DNA-mediated and other valence-limited colloidal interactions”,” *J. Chem. Phys.* **137**, 094108–094122 (2012).
- ²⁶P. Bolhuis, A. Louis, J. Hansen, and E. Meijer, “Accurate effective pair potentials for polymer solutions,” *The Journal of Chemical Physics* **114**, 4296–4311 (2001).
- ²⁷N. S. Bieler, T. P. Knowles, D. Frenkel, and R. Vácha, “Connecting macroscopic observables and microscopic assembly events in amyloid formation using coarse grained simulations,” *PLoS Comput Biol* **8**, e1002692 (2012).
- ²⁸L.-L. Pontani, I. Jorjadze, V. Viasnoff, and J. Brujic, “Biomimetic emulsions reveal the effect of mechanical forces on cell–cell adhesion,” *Proc. Natl. Acad. Sci. USA* **109**, 9839–9844 (2012).
- ²⁹L. Feng, L.-L. Pontani, R. Dreyfus, P. Chaikin, and J. Brujic, “Specificity, flexibility and valence of dna bonds guide emulsion architecture,” *Soft Matter* **9**, 9816–9823 (2013).
- ³⁰M. Hadorn, E. Boenzli, K. T. Sørensen, H. Fellermann, P. E. Hotz, and M. M. Hanczyc, “Specific and reversible dna-directed self-assembly of oil-in-water emulsion droplets,” *Proceedings of the National Academy of Sciences* **109**, 20320–20325 (2012).
- ³¹S. A. J. van der Meulen and M. E. Leunissen, “Solid colloids with surface-mobile dna linkers,” *J. Am. Chem. Soc.* **135**, 15129–15134 (2013), <http://pubs.acs.org/doi/pdf/10.1021/ja406226b>.
- ³²P. A. Beales and T. K. Vanderlick, “Application of nucleic acid–lipid conjugates for the programmable organisation of liposomal modules,” *Adv. Coll. Interf. Sci.* **207**, 290–305 (2014).
- ³³R. J. Banga, N. Chernyak, S. P. Narayan, S. T. Nguyen, and C. A. Mirkin, “Liposomal spherical nucleic acids,” *Journal of the American Chemical Society*, *Journal of the American Chemical Society* **136**, 9866–9869 (2014).

- ³⁴L. Parolini, B. M. Mognetti, J. Kotar, E. Eiser, P. Cicuta, and L. Di Michele, “Volume and porosity thermal regulation in lipid mesophases by coupling mobile ligands to soft membranes,” *Nat. Commun.* **6**, 5948 (2015).
- ³⁵E. Sackmann and A.-S. Smith, “Physics of cell adhesion: some lessons from cell-mimetic systems,” *Soft matter* **10**, 1644–1659 (2014).
- ³⁶L. Parolini, J. Kotar, L. Di Michele, and B. M. Mognetti, “Controlling self-assembly kinetics of DNA-functionalized liposomes using toehold exchange mechanism,” *ACS Nano* **10**, 2392–2398 (2016).
- ³⁷D. Frenkel, “Why colloidal systems can be described by statistical mechanics: some not very original comments on the gibbs paradox,” *Molecular Physics* **112**, 2325–2329 (2014).
- ³⁸S. Angioletti-Uberti, P. Varilly, B. Mognetti, A. Tkachenko, and D. Frenkel, ““Communication: A simple analytical formula for the free energy of ligand-receptor-mediated interactions”,” *J. Chem. Phys.* **138**, 021102–021106 (2013).
- ³⁹L. Di Michele, S. J. Bachmann, L. Parolini, and B. M. Mognetti, “Communication: Free energy of ligand-receptor systems forming multimeric complexes,” *J. Chem. Phys.* **144**, 161104 (2016).
- ⁴⁰D. T. Gillespie, “Exact stochastic simulation of coupled chemical reactions,” *The journal of physical chemistry* **81**, 2340–2361 (1977).
- ⁴¹P. Varilly, unpublished.
- ⁴²D. T. Gillespie, “Stochastic simulation of chemical kinetics,” *Annu. Rev. Phys. Chem.* **58**, 35–55 (2007).
- ⁴³M. Rathinam and H. El Samad, “Reversible-equivalent-monomolecular tau: A leaping method for small number and stiff stochastic chemical systems,” *Journal of Computational Physics* **224**, 897–923 (2007).
- ⁴⁴P. Grosfils, P. Gaspard, and T. V. de Bocarmé, “The role of fluctuations in bistability and oscillations during the h₂+ o₂ reaction on nanosized rhodium crystals,” *The Journal of chemical physics* **143**, 064705 (2015).
- ⁴⁵M. P. Allen and D. J. Tildesley, *Computer simulation of liquids* (Oxford university press, 1989).
- ⁴⁶P. Rossky, J. Doll, and H. Friedman, “Brownian dynamics as smart monte carlo simulation,” *Journal of Chemical Physics* **69**, 4628–4633 (1978).

- ⁴⁷E. M. Peck, W. Liu, G. T. Spence, S. K. Shaw, A. P. Davis, H. Destecroix, and B. D. Smith, “Rapid macrocycle threading by a fluorescent dye–polymer conjugate in water with nanomolar affinity,” *Journal of the American Chemical Society* **137**, 8668–8671 (2015).
- ⁴⁸D. Joshi, D. Bargteil, A. Caciagli, J. Burelbach, Z. Xing, A. S. Nunes, D. E. Pinto, N. A. Araújo, J. Bruijck, and E. Eiser, “Kinetic control of the coverage of oil droplets by dna-functionalised colloids,” arXiv preprint arXiv:1603.05931 (2016).

Appendix B: Supplementary Material: Bond formation kinetics affects self-assembly directed by ligand–receptor interactions

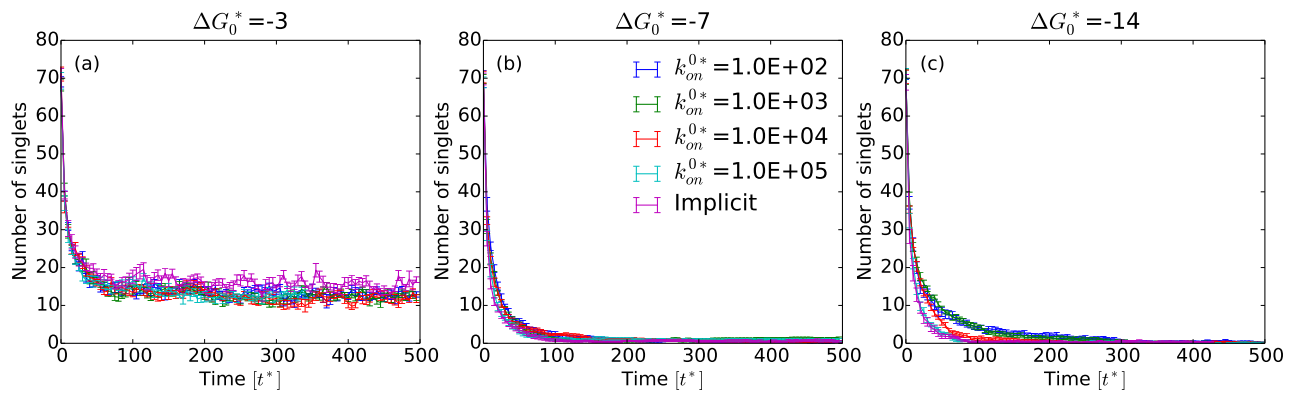


FIG. 8. Number of free particles *versus* simulation time at three different values of ΔG_0^* .

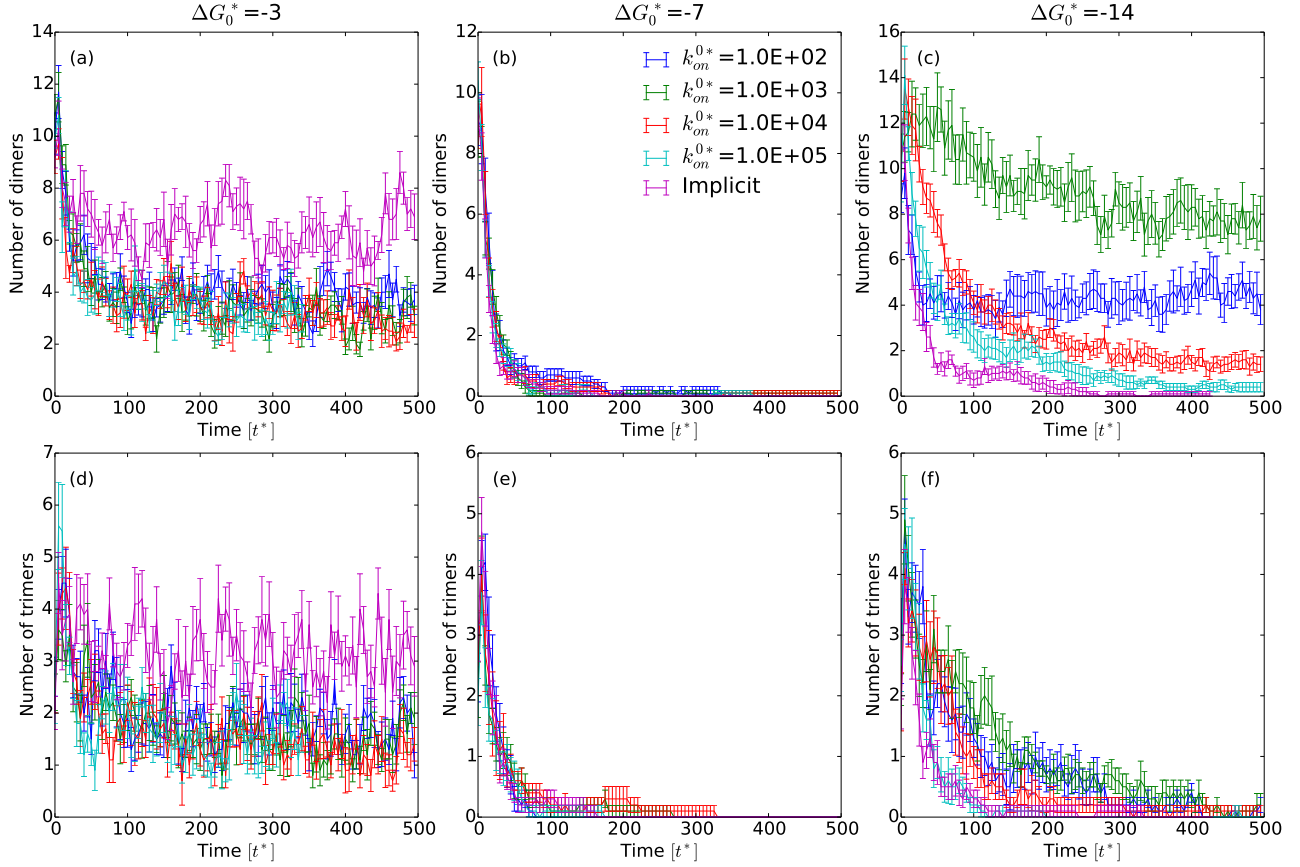


FIG. 9. Number of dimers (first row) and trimers (second row) *versus* simulation time at three different values of ΔG_0^* .

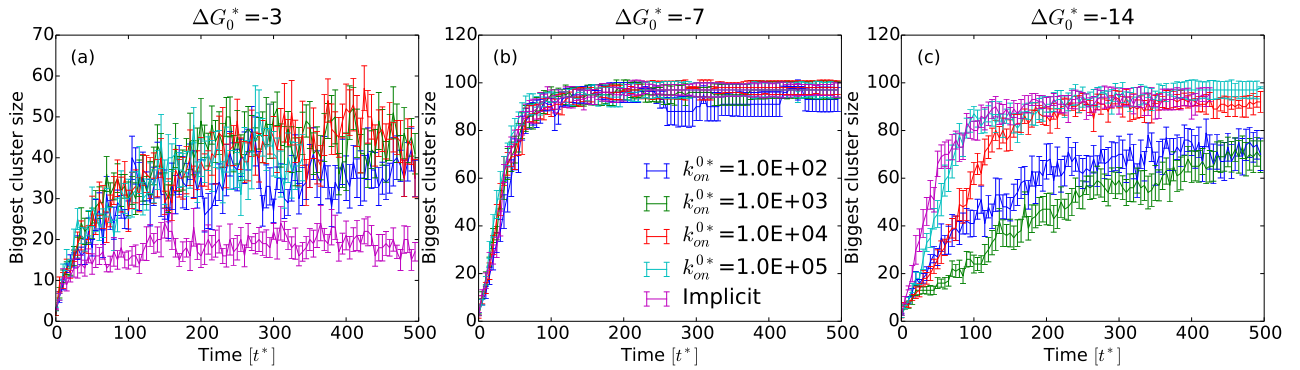


FIG. 10. Size of the biggest cluster in the system *versus* simulation time at three different values of ΔG_0^* .

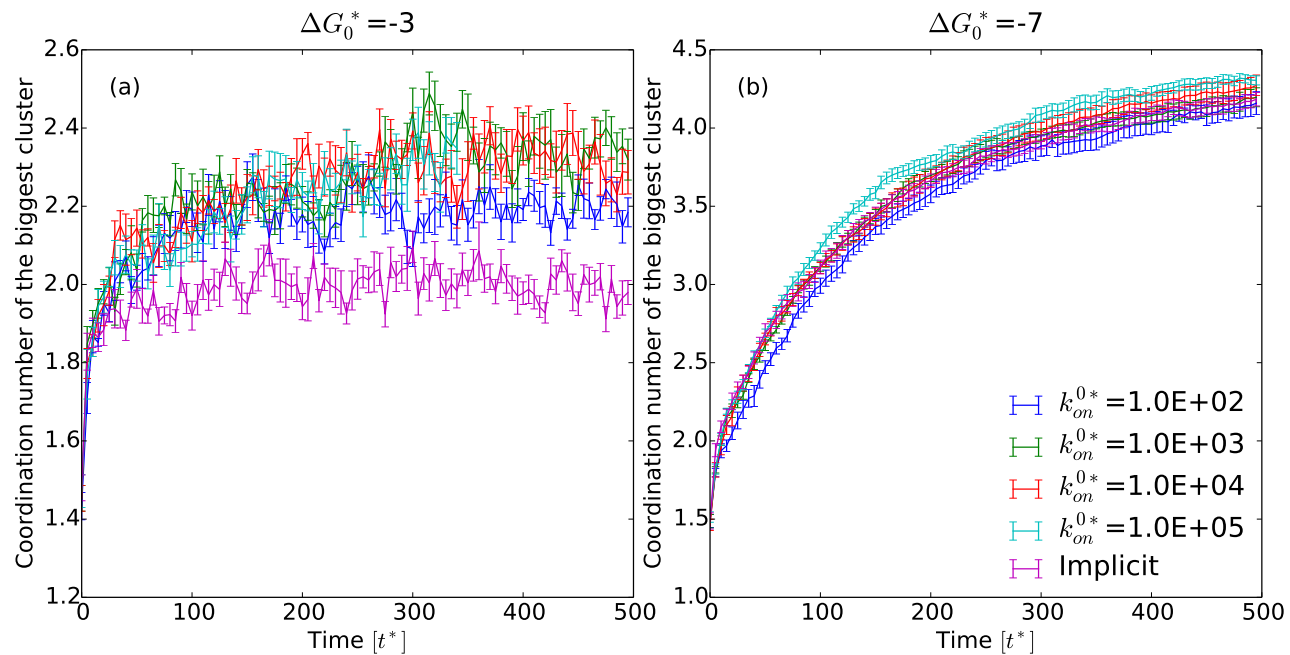


FIG. 11. Average valency ($\langle z \rangle$) of particles in the biggest cluster *versus* simulation time for two different ΔG_0^* .

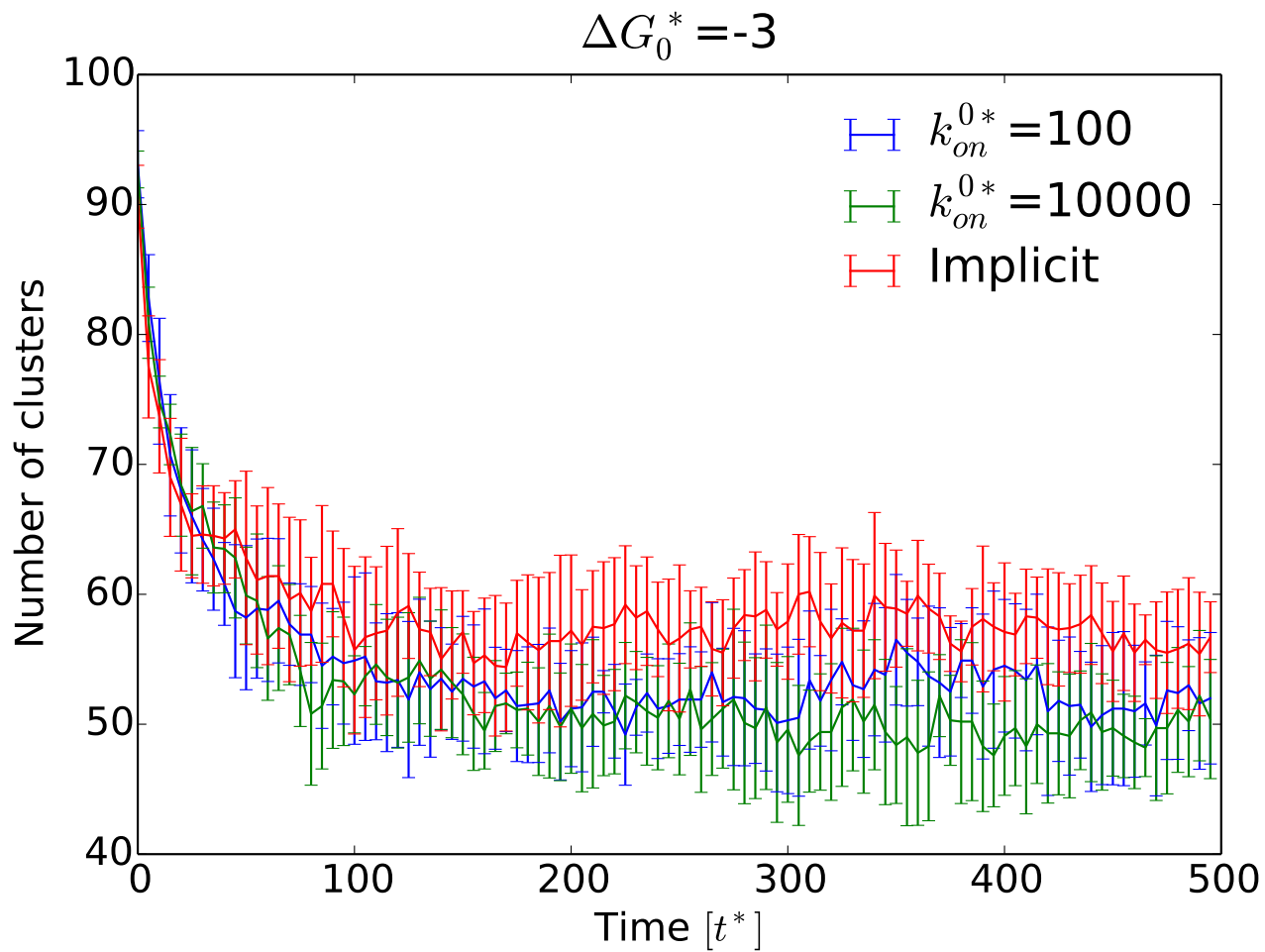


FIG. 12. Number of clusters *versus* simulation time at packing fraction 0.05 and $\Delta G_0^* = -3$.

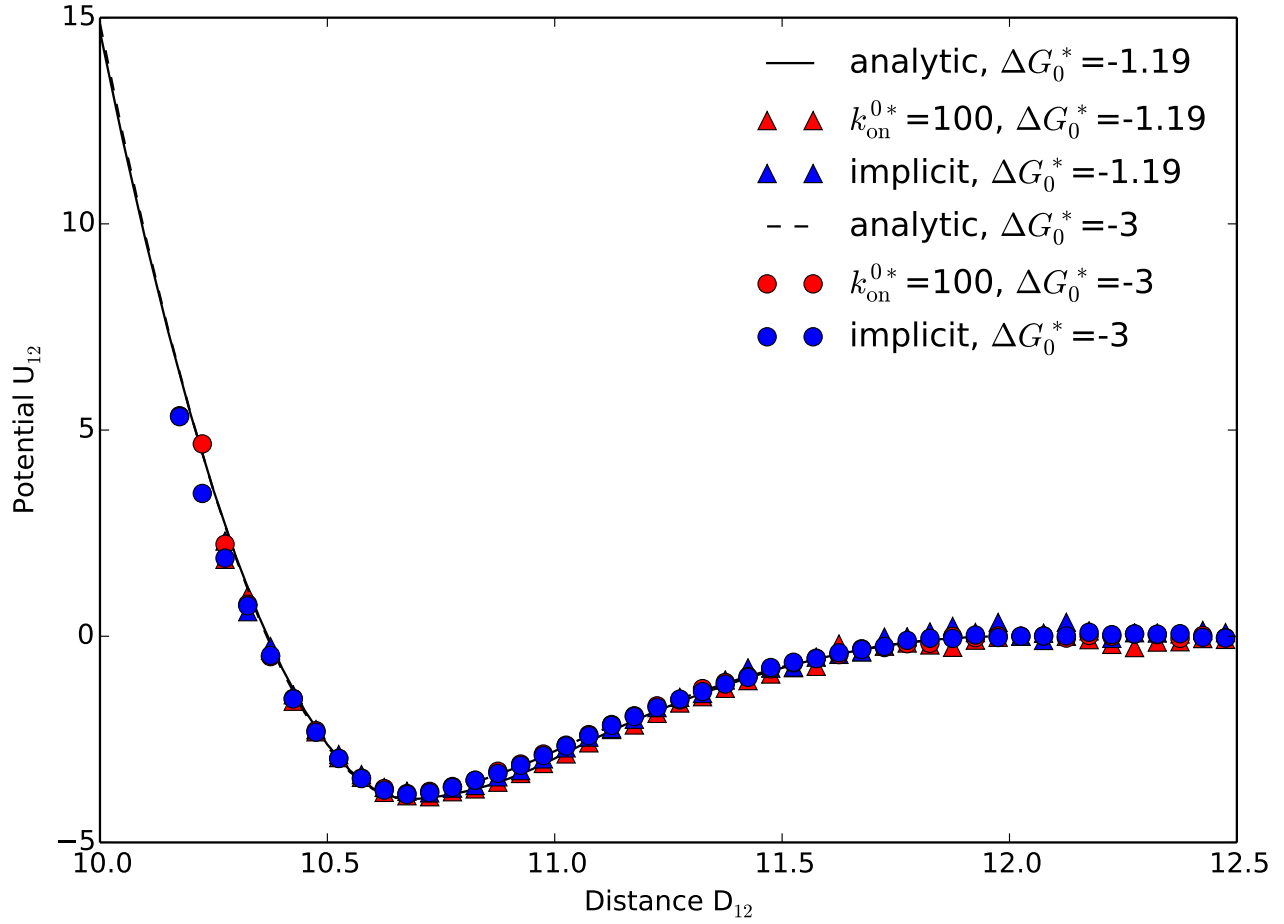


FIG. 13. Effective pair interaction as calculated using implicit-linker (blue symbols) and the explicit-linker method (red symbols) as a function of the distance between particle centres of mass (D_{12}). Curves refer to analytic predictions of U_{12} . Triangles refer to a system with $N = 100$ linkers and $\Delta G_0^* = -1.19$, while dots to a system with $N = 40$ and $\Delta G_0^* = -3$.

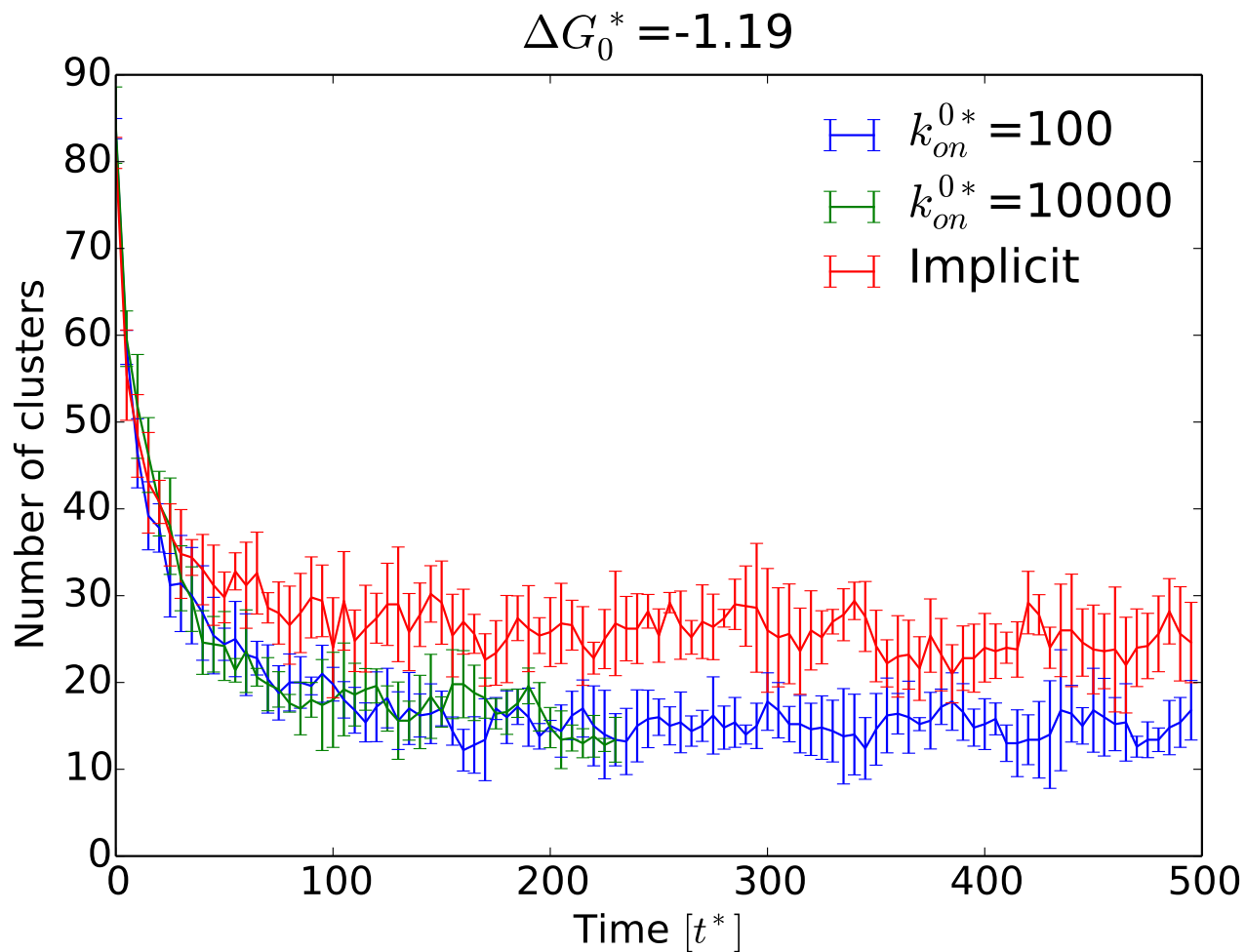


FIG. 14. Number of clusters *versus* simulation time for a model with $N = 100$ and $\Delta G_0^* = -1.19$.

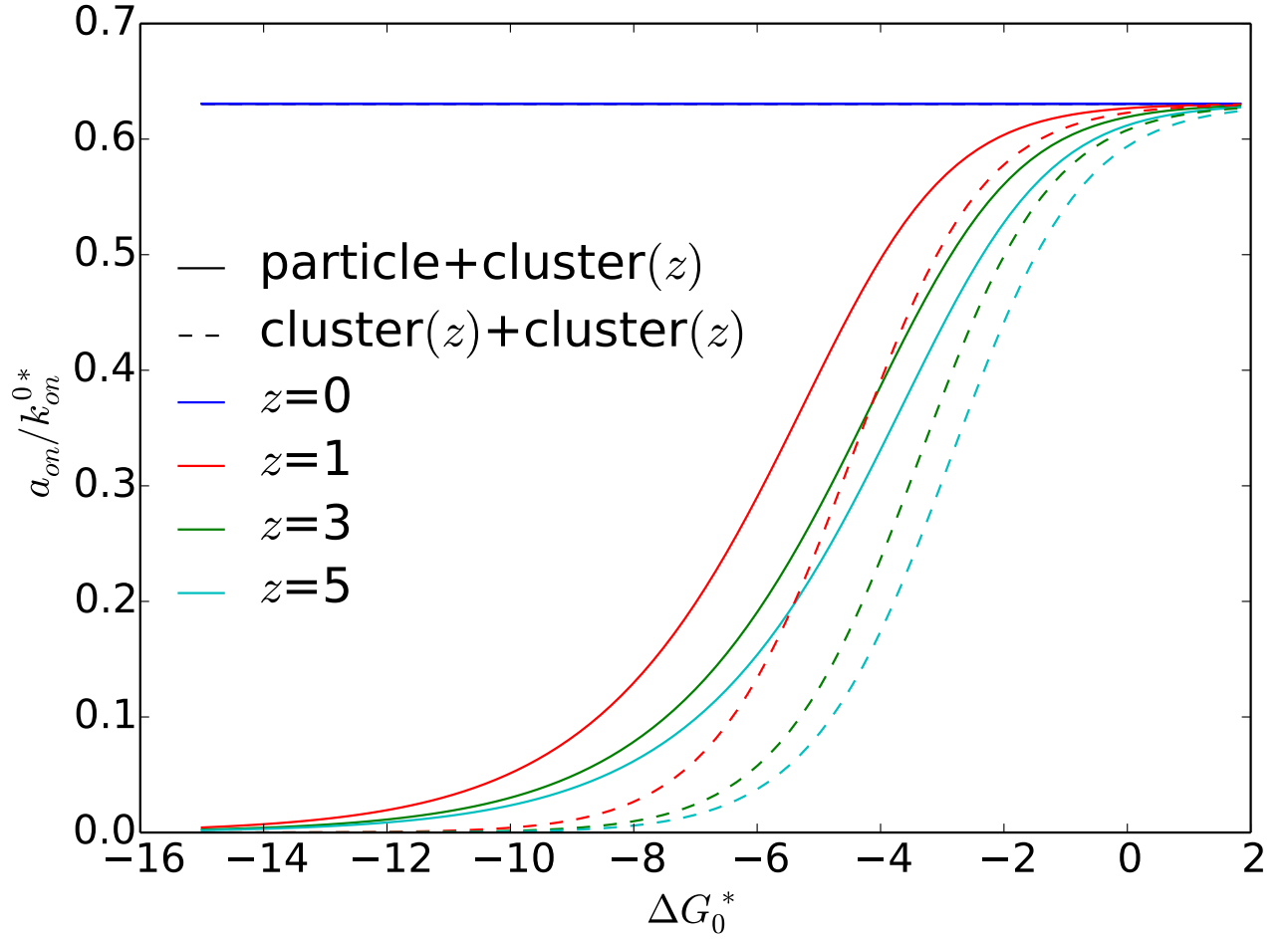


FIG. 15. Propensity (see manuscript Eq. 9) of attaching an isolated particle to an existing cluster (solid lines), and propensity of creating a new linkage between two particles embedded in the same cluster (dashed lines). If compared to manuscript Fig. 6 the number of linkers was increased from $N = 40$ to $N = 100$. In all calculations the distance between linkable particles has been taken equal to $2 \cdot R + L$ and z is the cluster coordination number.